Lecture 10.

Prediction of Welding Distortion

A two-step numerical analysis technique was developed to predict welding-induced distortion and the structural integrity of large and complex structures

BY P. MICHALERIS AND A. DEBICCARI

ABSTRACT. This paper presents a numerical analysis technique for predicting welding-induced distortion. The technique combines two-dimensional welding simulations with three-dimensional structural analyses in a decoupled approach. The numerical technique is particularized on evaluating welding-induced buckling. The numerical predictions can be utilized either as a design evaluation or manufacturing analysis tool. As a design tool, the effect of the welding procedures can be determined and incorporated into the evaluation and optimization of the design configurations. As a manufacturing analysis tool, for a fixed design, different welding processes and procedures can be evaluated to minimize welding distortion. Experimental results obtained from small- and large-scale mock-up panels verify the numerical modeling approach.

Introduction

Conventional design methodologies either ignore or use empirical techniques to evaluate the effects of welding on the structural integrity and dimensional control of welded structures. To efficiently assess the effects of welding on structural performance and effectively implement various mitigation techniques to control or counteract welding distortion, a methodology for predicting the distortion due to welding is necessary.

Masubuchi (Ref. 1) discusses the various types of welding-induced distortion, including control and mitigation techniques. In thin-section structures as frequently used in the shipbuilding, railroad, aerospace and automotive industries, buckling is a common type of distortion. When it occurs, the magnitude of distortion tends to be very large. Furthermore, buckling instabilities reduce the structural integrity of a welded structure. Use of predictive analysis tools can determine the susceptibility of a design to the various types of distortion and assist the selection of geometry configuration and manufacturing processes that minimize distortion.

Currently, control of weld distortion is implemented empirically with experiments performed under a range of conditions. The experimental results are used to develop correlations parametrizing the effects of various welding and geometric factors and then establish sets of welding procedures that allow for the production of acceptable structures (Ref. 2). These types of experimentally derived criteria are applicable only for the tested range of geometric configurations and welding conditions. To evaluate modified geometries and conditions, additional tests are required. Masubuchi (Ref. 1) presents simplified closed form analytical solutions for the evaluation of welding conditions susceptible to buckling, but these solutions are available only for simplified geometries (*i.e.*, no stiffeners).

Over the past 15 years, the finite element method has been used in an attempt to predict distortion and residual stress due to welding (Refs. 3–10). More recent developments involve the inclusion of phase transformations and transformation plasticity in the analyses (Refs. 11–14). The majority of these simulations focuses on simple structural components in the area immediately adjacent to the weld and investigates residual stress, local distortion and microstructure.

KEY WORDS

Distortion
Buckling
Finite Element Analysis
2-D Welding Simulations
3-D Structural Analysis
Eigenvalue Analysis
Thin-Panel Fabrication

Brown and Song (Ref. 15) show that the interaction between the weld zone and the structure can have a dramatic effect on the accumulated distortion. In many cases, the contribution of the structure dominates the state of distortion and stress, a state that is much different from the one predicted by a simulation of the weld zone alone. Some distortion modes, most notably buckling caused by longitudinal stresses, cannot be represented by two-dimensional models in the plane perpendicular to the welding direction. However, the use of a fully three-dimensional model to perform the thermomechanical weld simulations of complex structures is impractical and computationally prohibitive. Daniewicz (Ref. 16) presents a hybrid (experimental-numerical) approach to predict weld distortion of large offshore structures. The weld joints are represented by "weld elements" to simulate the shrinkage caused by welding, which is determined experimentally. The approach yields only quantitatively accurate results, which can be attributed to the experimental determination of weld shrinkage.

This paper presents a two-step numerical analysis technique for predicting welding-induced distortion and assessing the structural integrity of large and complex structures. The technique combines two-dimensional welding simulations with three-dimensional structural analyses in a decoupled approach. The predicted residual stress from a two-dimensional welding simulation is used to determine the loading for the three-dimensional structural analysis, which can include elastic buckling and/or large deformation analyses. The two-dimensional welding simulations ensure that the welding load of the structural analysis is determined accurately in a predictive manner using limited computer resources. The structural analyses simulate the response of the large structure, including instabilities such as buckling.

The numerical methodology is applied on stiffened panel structures and particularized on evaluating welding-induced buckling. Experimental results ob-

PANAGIOTIS MICHALERIS and ANDREW DEBICCARI are with the Edison Welding Institute, Columbus, Ohio.
Paper presented at the AWS Annual Convention, April 1996, Chicago, ILL.

up shipbuilding panels are used to verify the predictive methodology.

Distortion Prediction

Decoupling of Welding Simulation and Structural Analysis

Welding in large unrestrained structures can cause significant distortions in modes that simplified two-dimensional analyses of the weld region may not capture (Ref. 15). Specifically, the parts may move relative to each other and the weld may be placed in a different location than that of the undeformed configuration. This type of response necessitates the use of fully coupled three-dimensional thermomechanical analyses. In general welding practice, however, the parts are tack welded and/or mechanically restrained prior to welding. Therefore, the parts stay stationary relative to each other and the welds are placed on the predetermined configuration, relaxing the fully coupled requirement.

Two-dimensional models on the plane perpendicular to the welding direction offer good residual stress approximations for continuous welds of relatively high weld speeds (Refs. 4, 5, 17). Large structures, however, may buckle due to residual stresses parallel to the welding direction. In a section perpendicular to the welding direction, the longitudinal stresses during welding are compressive at the weld zone and tensile elsewhere. This stress state is not susceptible to buckling. As the section cools down, the stress pattern reverses and buckling may occur. Furthermore, most of the plastic deformations occur during welding and only in the vicinity of the weld region. Therefore, the structural response of a large structure to welding may be evaluated in two steps. First, a two-dimensional welding simulation can be performed to determine the residual stress distribution. The model may be limited to a portion of the structure that represents the mechanical restraints that are used. Then a three-dimensional structural (elastic) analysis can be performed using the stress distribution of the welding simulations as loading to determine if the structure will buckle and the corresponding mode and/or magnitude of deformation.

The advantage of a decoupled approach is computational simplicity and efficiency. Complex three-dimensional welding simulations are not performed. Moreover, for several weld sizes or heat inputs, the residual stresses, which here are considered as loads on a structure, can be computed independently from the structural response. The approach allows the evaluation of the initial design and following modifications without the need of performing any additional welding simulations.

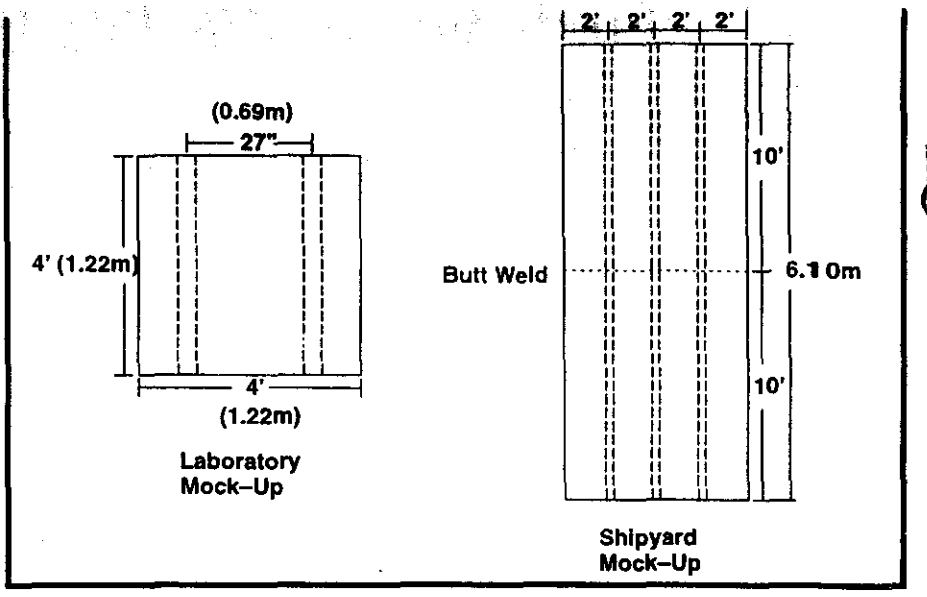

Fig. 1 — Experimental mock-up configurations.

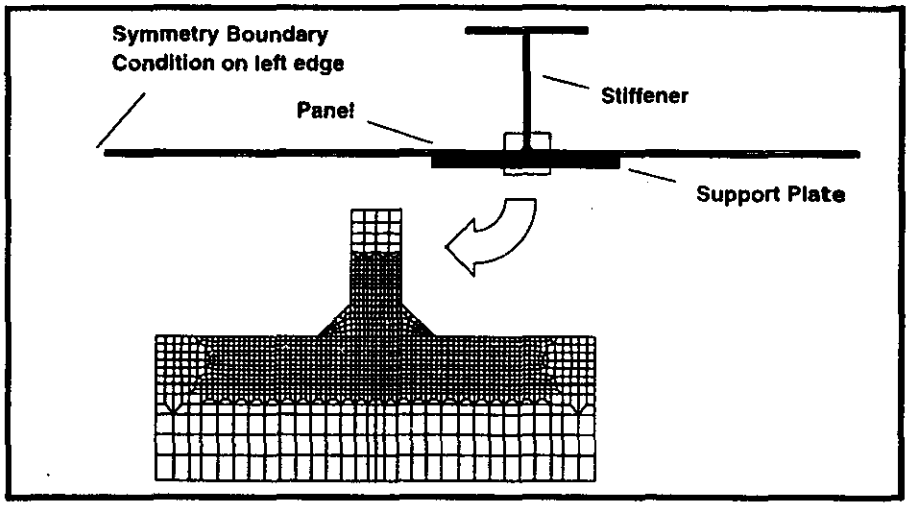

Fig. 2 — Finite element analysis mesh of welding simulations.

Welding Simulation

Two-dimensional thermomechanical welding simulations are performed to determine the residual stresses. The welding simulations follow the work of previous investigators (Refs. 4, 5, 17). Phase transformations are not considered in this study.

Structural Analysis

To evaluate the response of a welded structure, elastic small deformation, eigenvalue and incremental large deformation analyses are considered. A small deformation analysis assumes that the displacements are infinitesimal and that the loads are applied on the undeformed geometry. Small deformation analyses require limited computational resources, cannot account for buckling behavior, and are used in this work only to scale the weld load from a welding simulation to the structural analysis. Eigenvalue analyses here refer to the elastic instability problem defined as follows:

$$\det(\mathbf{K} + \lambda \mathbf{K}_G) = 0 \qquad (1)$$

where $\mathbf{K}$ and $\mathbf{K}_G$ are the linear and nonlinear strain stiffness matrices, respectively (Refs. 18, 19). Eigenvalue analyses are easy to implement and are used here to provide an estimate of a structure's critical buckling load and its distorted shape. Incremental large deformation analyses determine both the critical buckling load and distortion magnitude accurately. However, they are computationally in-

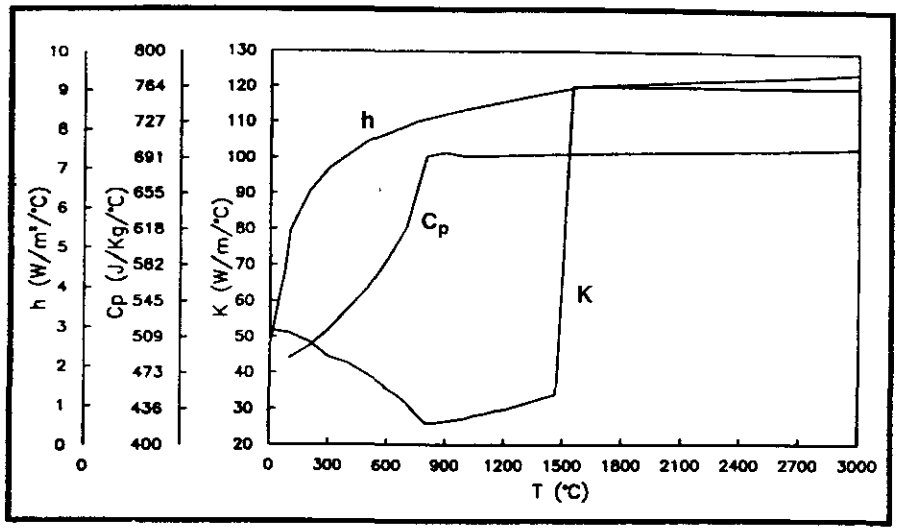

Fig. 3 — Thermal conductivity, specific heat and convection coefficient.

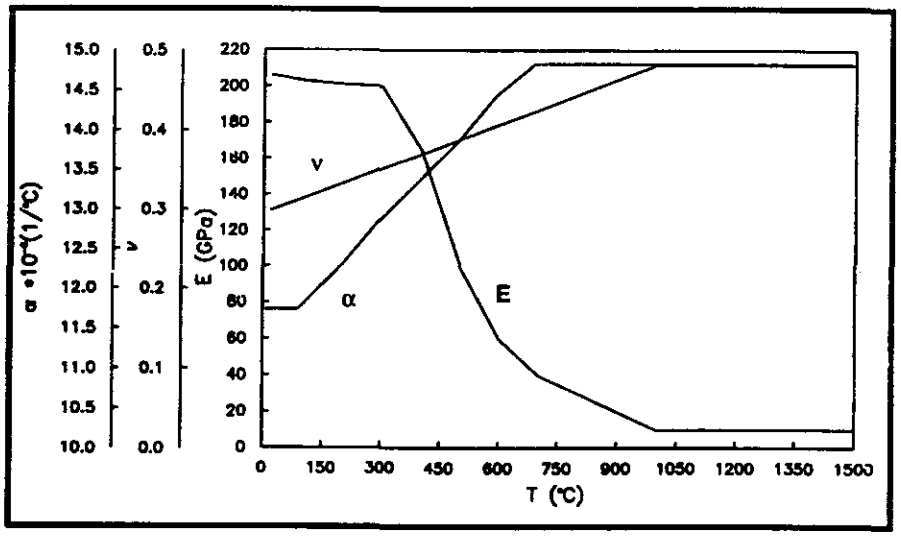

Fig. 4 — Young's modulus, Poisson's ratio and thermal expansion coefficient.

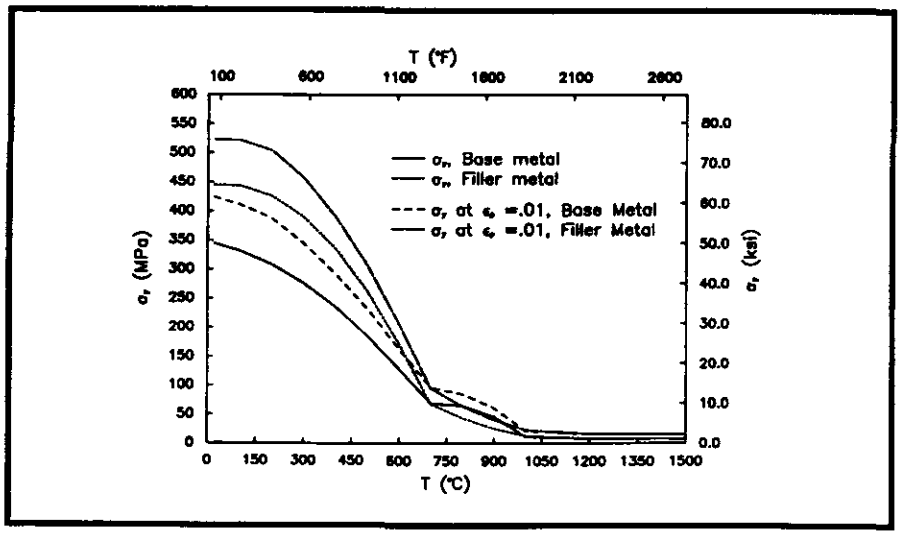

Fig. 5 — Yield strength.

tensive and so are used only to further validate the predictive methodology.

Implementation and Experimental Verification

The decoupled computational approach is implemented on welding of stiffened panels typical of those used in shipbuilding. The methodology is presented as applied in the determination of the welding conditions that cause buckling of the panels. Finite element analyses and corresponding experiments are performed to investigate the development of distortion and verify the computational approach. The experimental measurements focus on verifying the accuracy of the welding simulation, the ability to predict the conditions that cause buckling and the ability to predict the distortion magnitude. Additional details on the experimental procedures are presented in Condardy (Ref. 20). Both small (laboratory) and large (shipyard) scale mock-up panels made of AH-36 steel are used in the experimental study. The use of two panels sizes is necessary to ensure the scalability of results.

A panel thickness of 3/16 in. (4.7625 mm) is selected, as this thickness is observed in shipyards to have the most distortion. The size of the panels is set to 4 x 4 ft (1.22 x 1.22 m) for laboratory mock-ups and 20 x 8 ft (6.10 x 2.44 m) for the shipyard mock-ups. The shipyard panels are constructed by butt joint welding two 10 x 8 ft plates together. The longitudinal stiffener size is 4 x 4 in. x 5 lb, which is typical for panels of this thickness. The longitudinal stiffener spacing for the laboratory and shipyard mock-ups is 27 in. (685.8 mm) and 24 in. (609.6 mm), respectively. Typically, stiffened panels also contain transverse stiffeners along with the longitudinals. However, early experiments concluded that inclusion of the transverse stiffeners was unnecessary to study buckling. The resulting mock-up panel geometries are illustrated in Fig. 1.

Typical welding procedures are used to fillet weld the longitudinal stiffeners to the panels. Double fillet welds are produced automatically using the flux cored arc welding process. Nominal longitudinal stiffener fillet weld sizes for 1/16-in.-thick panels are selected, with fillet leg lengths ranging from 1/8 to 3/16 in. (3.175 to 4.7625 mm). These size welds correspond to heat inputs of 7.8–18.2 kJ/in. (307.1–717 J/m) per torch. The torches are offset by 3.5 in. (88.9 mm).

Welding Simulations

Thermal Analysis

Two-dimensional nonlinear transient heat flow finite element analyses are per-

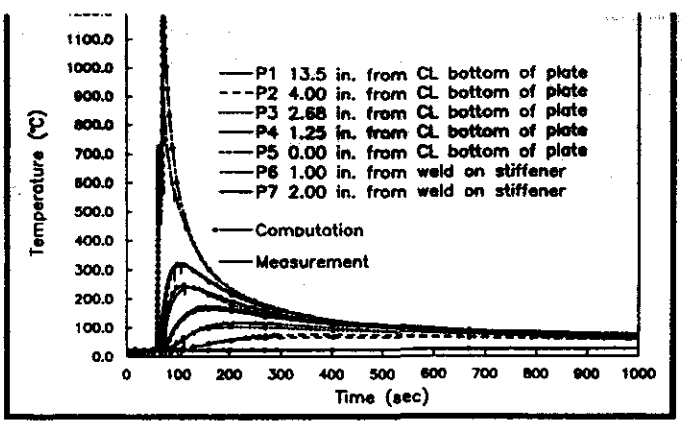

Fig. 6 — Correlation of temperature history for 18.2 kJ/in. (717 J/m) welds.

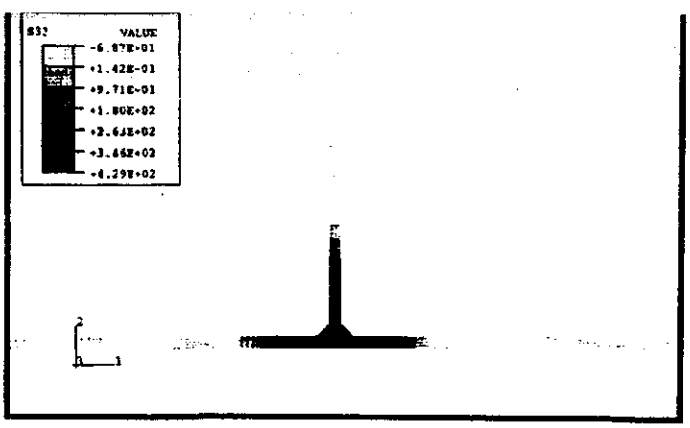

Fig. 7 — Contour plot of longitudinal residual stress (MPa) for 18.2 kJ/in. (717 J/m) welds.

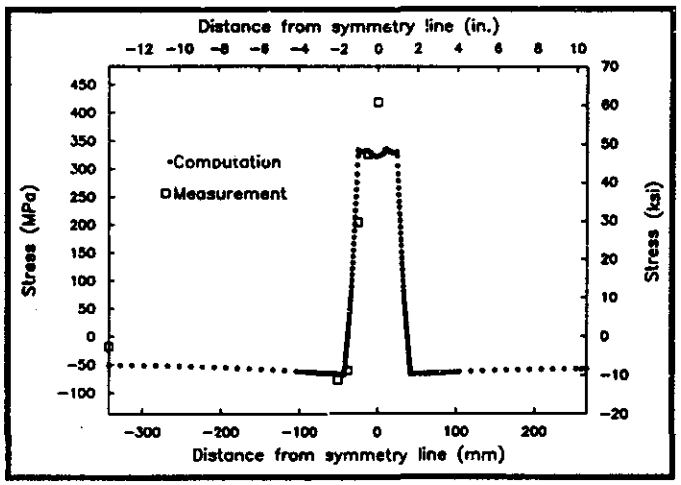

Fig. 8 — Correlation of longitudinal residual stresses on bottom surface for 18.2 kJ/in. (717 J/m) welds.

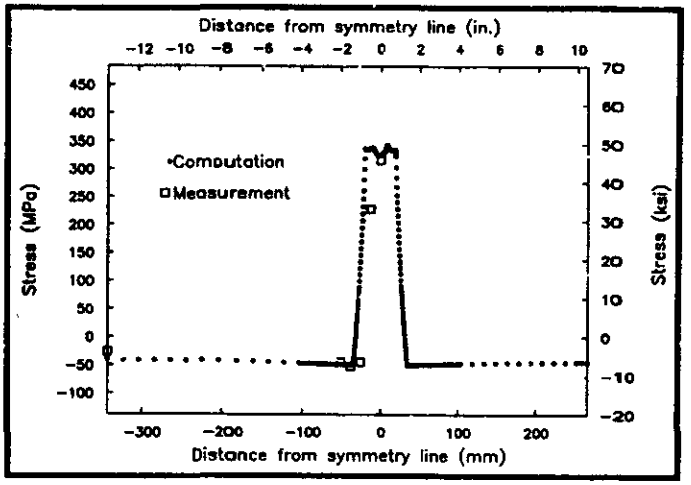

Fig. 9 — Correlation of longitudinal residual stresses on bottom surface for 10.2 kJ/in. (402 J/m) welds.

formed in the plane perpendicular to the welding direction. Figure 2 illustrates a typical model, consisting of 9338 nodes and 3018 elements. Heat conduction, quadratic, quadrilateral elements (ABAQUS DC2D8) are used. The stiffener web and flange are assumed to be of a uniform 3/16-in. (4.7625-mm) thickness. To simulate the heat losses to the support during welding, a support plate connected to the panel with gap conductivity elements (ABAQUS DINTER3) is added in the model. The gap conductivity is back-calculated for each case investigated to correlate computed temperatures to measured values. For simplicity, the criterion for the back calculation is a visual best fit.

The heat generated by the welding process is modeled with a "double ellipsoid" heat source model (Ref. 17) for each fillet, where the heat generated by welding is simulated with a power density moving along with the torch. Radiation and convection boundary conditions are assigned for all free surfaces. A temperature-dependent free convection coefficient is used here and is plotted in Fig. 3 (Ref. 15). The emissivity is set to 0.2 (Ref. 15). Material properties for mild steel (*i.e.*, SAE 1020) are used in this study because minor variations in alloy content for structural steels have negligible influence on these properties. The temperature-dependent thermal conductivity K, and specific heat C_p are also plotted in Fig. 3 (Ref. 21). The thermal conductivity is increased artificially for temperatures above the melting point to simulate the convective heat transfer of the weld pool (Refs. 4, 17). The latent heat of fusion is set to 247 kJ/(kg•°C) (Ref. 22) and the density to 7.86 x 103 kg/m³ (Ref. 21).

Mechanical Analysis

Generalized plane strain, quasi-static finite element analyses are performed using ten node, quadratic, reduced integration, quadrilateral elements (ABAQUS CGPE10R). The mesh is identical to that used for the thermal analysis, excluding the support plate. Symmetry boundary conditions are used on the left edge of all models — Fig. 2.

Elastic-plastic material response is assumed with kinematic work hardening. Figures 4 and 5 illustrate the temperature-dependent mechanical properties. All mechanical properties except yield strength are those of mild steel, again because minor variations in alloy content for structural steels have negligible influence on these properties. The plastic hardening modulus is taken from Mizukami (Ref. 23). All other properties are taken from Goldak (Ref. 24).

Results and Verification

Thermocouple measurements are

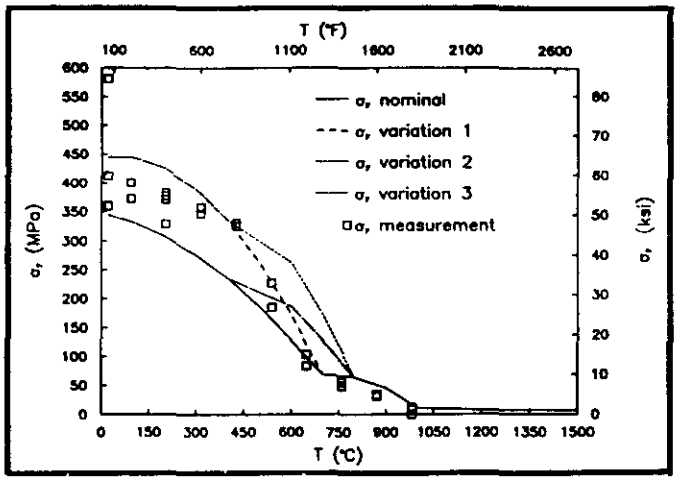

Fig. 10 — Yield strength sensitivity analysis.

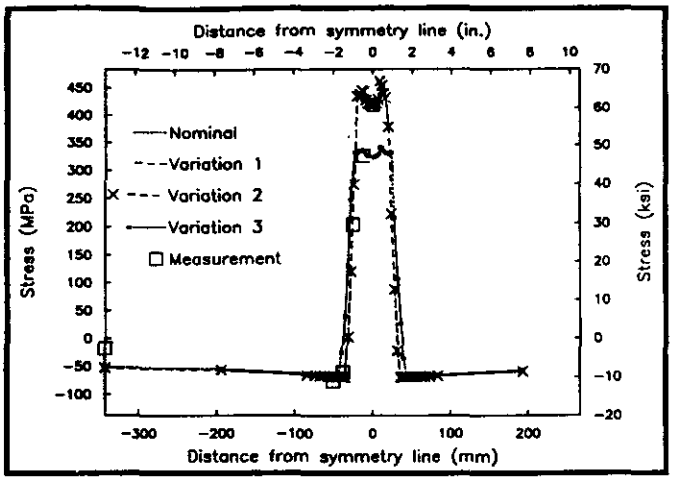

Fig. 11 — Longitudinal residual stress variations with yield strength for 18.2 kJ/in. (717 J/m) welds.

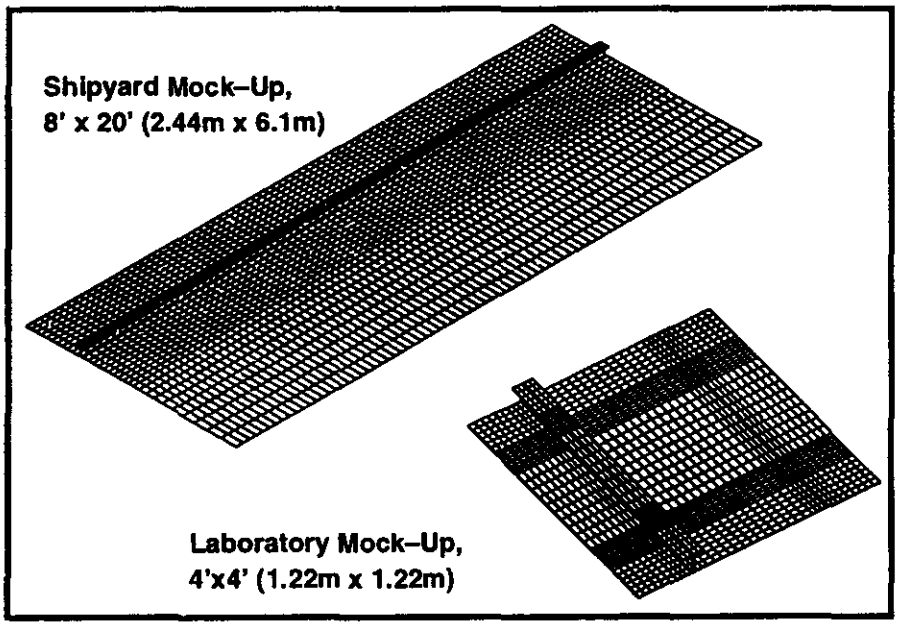

Fig. 12 — Finite element models of mock-ups.

performed to determine the gap conductance of the interface elements (Fig. 2) and to verify the thermal analysis. Figure 6 illustrates the correlation of computed and measured temperatures for the 18.2 kJ/in. per torch fillet welds. Since the gap conductivity is adjusted to obtain the best fit of computed and measured temperatures, the correlation of Fig. 6 verifies the analyses only in the sense that a set of transient measurements at several locations is matched by varying one variable — the gap conductivity. In general, good agreement is obtained with the exception of temperatures at the weld region, which are slightly overpredicted. This observation is consistent with the use of a two-dimensional model, which does not consider the heat flow in the welding direction (Ref. 25). The correlations for other weld heat inputs are similar.

Figure 7 illustrates the computed longitudinal residual stress distribution for the 18.2 kJ/in. fillet welds. At the weld region, the residual stresses are tensile and of yield magnitude. At locations remote to the weld, compressive residual stresses are developed, equilibrating the tensile stresses of the weld zone. Surface residual stress measurements by the blind hole drilling method verify the computations. Figures 8 and 9 present correlations of computed and measured residual stresses for the 18.2 and 10.2 kJ/in. heat input welds, respectively. Good agreement is observed. Furthermore, the simulation correctly predicts the size of the area under tensile residual stress. The correlations for other weld heat inputs are similar. Finally, the experimental results confirm that the longitudinal residual stress distribution is independent of the panel size, validating the generalized plane strain assumption.

Solution Stability

Sensitivity analyses are performed to determine the stability of the solution with respect to variations of the geometry and the material properties. The welding simulation is repeated on a modified stiffener geometry reflecting typical variations in stiffener dimensions. A comparison of the resulting residual stress profiles shows them to be virtually identical.

The most sensitive material property to alloy content and process variations is the yield strength. The temperature-dependent yield strength used in the welding simulations (Fig. 5) is the specified minimum for AH-36, which for room temperature is 345 MPa (50 ksi). However, the actual plates used in this investigation exceed the specified minimum yield strength as shown in Fig. 10. The effect of these differences on the results of the welding simulation is investigated by performing analyses for three different variations on the yield strength vs. temperature shown in Fig. 10. In variation 1, the room temperature yield strength is increased from 345 to 445 MPa (50 to 64 ksi) (30%). In variation 2, the yield strength at both room temperature and elevated temperatures (450–800°C (842–1472°F)) is increased, and in variation 3, the yield strength is increased only at elevated temperatures. The corresponding residual stresses for an 18.2 kJ/in. weld are illustrated in Fig. 11. As seen in the figure, variations of the yield strength at elevated temperatures have no effect on the computed residual stress profile. However, increasing the room temperature yield strength decreases the width and increases the magnitude of the

quence, the compressive stress between stiffeners increases from 51.2 to 53.0 MPa (7.42 to 7.69 ksi) (3.6%).

Buckling Prediction

To assess a structure's propensity to buckle under a given set of welding conditions, the structure's critical buckling load is compared to the applied load as induced by the welding residual stresses. Three-dimensional finite element models of the laboratory and shipyard mock-ups are evaluated using both continuum and structural models.

Continuum Model

The continuum models consist of 20 noded reduced integration elements (ABAQUS C3D20R) representing the plate and stiffener, and 15 noded prism elements (ABAQUS C3D15) representing the fillet welds. Each model contains only one stiffener, as both initial numerical and experimental tests indicate that buckling occurs during the welding of the first stiffener. The finite element models are illustrated in Fig. 12. The laboratory mock-up model consists of 2508 elements and 18,019 nodes, while the shipyard mock-up consists of 4160 elements and 28,903 nodes. Constant room temperature material properties are used, with an Elastic Modulus of 30.0 x 10^6 psi (206.9 GPa) and Poisson's ratio of 0.29. On the shipyard panel, one foot at each end of the stiffener is left unconnected to represent the "leave loose" condition employed at the shipyard. The models are constrained by assuming that the out-of-plane displacement of the base plate directly under the stiffener is restricted by the stiffener's weight. To allow bending of the stiffener, this constraint is imposed only directly beneath the stiffener's ends. In-plane displacements are not restricted except as necessary to remove rigid body motions.

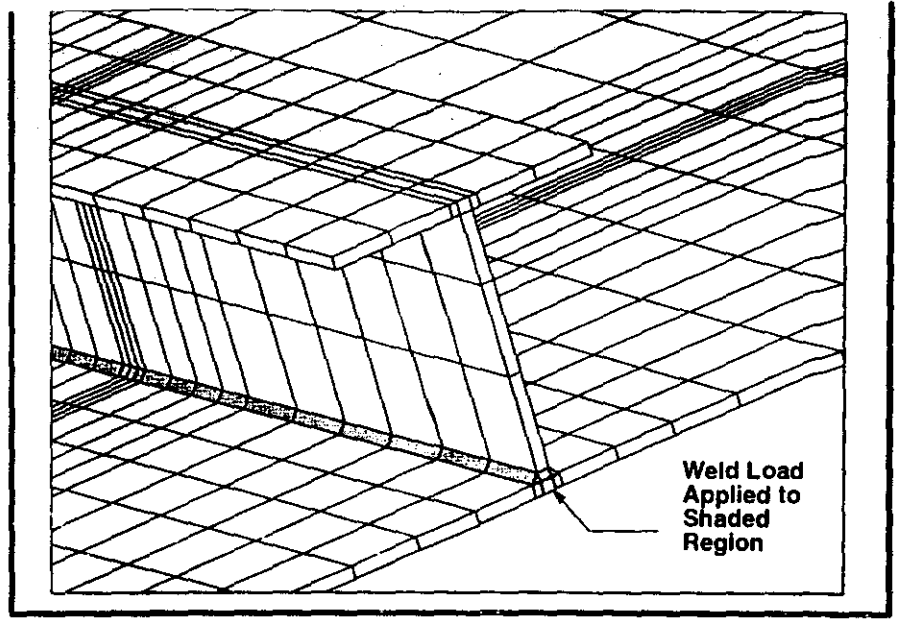

Fig. 13 — Weld load application area.

Applied Weld Load

The computed residual stress field from the welding simulation is applied as loading on a structural analysis. Rather than a direct mapping of residual stress that would require the use of complex routines and limit implementation, a simplified methodology is developed here.

To develop a stress field similar to the one computed by the welding simulation, the weld region is subjected to a thermal loading. Similar residual stress distributions can be generated by imposing a strain as load. A thermal load is used here as it is easily applied in the finite element code used (ABAQUS). The loaded area is illustrated in Fig. 13. A combination of orthotopic thermal expansion coefficients and a uniform temperature load is used. The use of orthotopic properties allows for different levels of loading in the longitudinal and transverse directions. In this study, only the thermal expansion coefficient in the weld direction is nonzero. A value of 1.0 x 10^{-5} in./(in.•°F) (5.6 x 10^{-6} m/(m•°C) is used. Further studies are planned to include the effect of angular distortion by using nonzero thermal expansion coefficients in additional directions.

To determine the weld load, the resulting longitudinal residual stress pre-

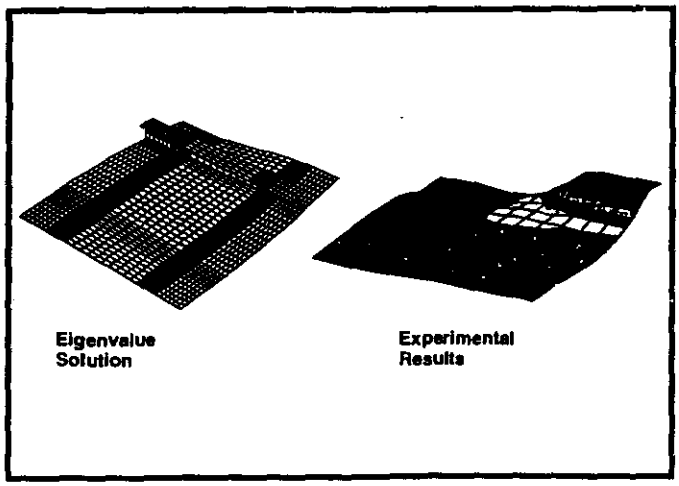

Fig. 14 — Comparison of predicted mode shape and experimental results for laboratory mock-up.

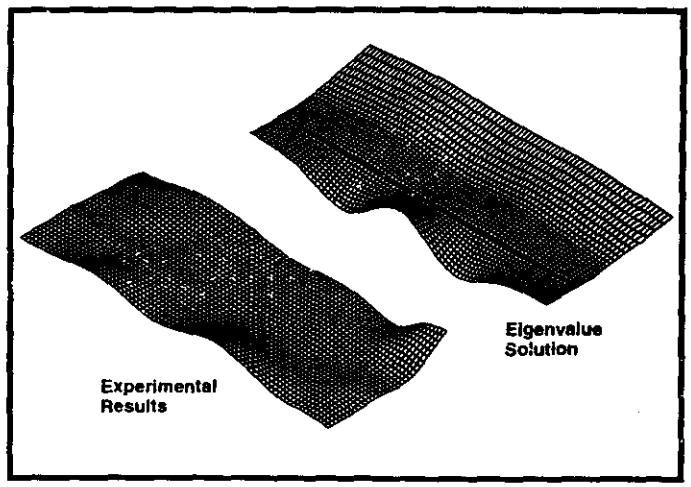

Fig. 15 — Comparison of predicted mode shape and experimental results for shipyard mock-up.

Table 1 — The Comparison between the Predicted and Observed Results for the Continuum Model

Panel Size (ft)	Plate Thickness (in.)	Heat Input per Torch (kJ/in.)	Nominal Weld Size (in.)	Applied Weld Load AWL (lb)	Critical Buckling Load CBL (lb)	Buckling Predicted	Buckling Observed
4 × 4	3/16	7.88	1/8	23,902	35,248	No	No
4 × 4	3/16	10.2	5/32	31,736	36,740	No	No
4 × 4	3/16	18.2	3/16	40,929	36,439	Yes	Yes
8 × 20	3/16	9.9	5/32	30,936	18,067	Yes	Yes
8 × 20	7/32	9.9	5/32	30,936	22,815	Yes	Yes

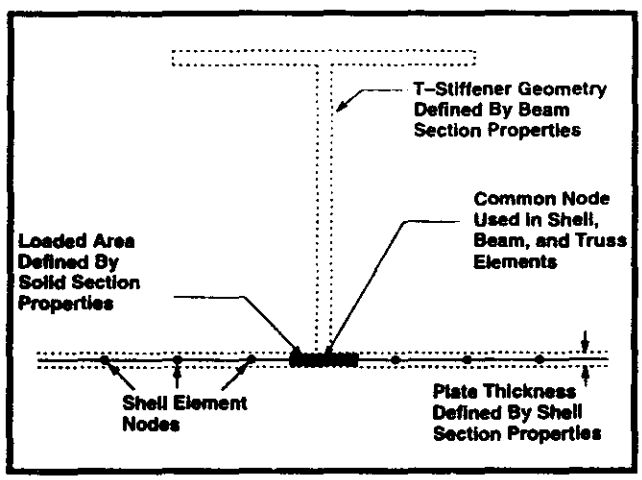

Fig. 16 — Schematic of stiffened panel model using shell, beam and truss elements.

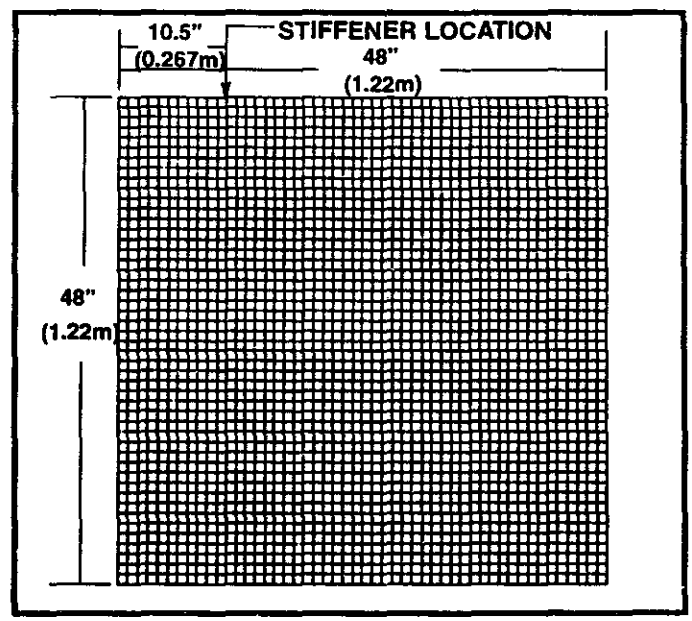

Fig. 17 — Finite element model for structural analysis of 4 x 4-ft (1.22 x 1.22-m) mock-up.

dictions from the weld simulation analyses are compared to a small deformation elastic analysis performed on the continuum model with a known thermal load. A small deformation analysis is implemented here because it does not account for buckling, which is consistent with the two-dimensional (2-D) welding simulation. The longitudinal compressive stress at the plate mid-span resulting from the thermal load is then compared to the compressive residual stress predicted by the weld simulation analysis. Since the small deformation analysis is linear, the applied thermal load necessary to match the predicted residual stress, ΔT_{APP}, is easily obtained by scaling the thermal load as follows:

$$\frac{\Delta T_{APP}}{\Delta T_1} = \frac{\text{Residual stress at plate midspan from 2D analysis}}{\text{Stress at plate midspan in 3D model under load } \Delta T_1} \quad (2)$$

where ΔT_1 is a unit temperature load.

In an effort to define a load scale independent of the material properties used and the area where the thermal load is applied, the applied weld load (AWL) is defined as the product of the elastic modulus E, applied load cross-sectional area A, thermal expansion coefficient α, and temperature loading ΔT_{APP}:

$$AWL = EA\alpha\Delta T_{APP} \quad (3)$$

The calculated AWL values for the weld simulation analyses performed are listed in Table 1.

Critical Buckling Load

The panel's critical buckling load under welding is determined by an eigenvalue analysis. A unit temperature load of $\Delta T_1 = -1°F$ (0.56°C) is imposed over the weld load application volume — Fig. 13. The panel's critical buckling load CBL is then defined as

$$CBL = \lambda EA\alpha\Delta T_1 \quad (4)$$

where λ is the minimum positive eigenvalue. The corresponding eigenmode for each eigenvalue represents the distorted shape of the panel.

Table 1 contains the computed CBL for various panel geometries. The table shows that for a given plate thickness, the CBL is insensitive to weld size. Although the eigenvalues are different, they are inversely proportional to the loaded cross-sectional area, so the product $\lambda EA\alpha\Delta T_1$ remains relatively constant. This is due to the fact that the change in the overall structural stiffness with respect to weld size is negligible. For a given weld size, however, the critical buckling load increases with plate thickness. Furthermore, an increase in plate thickness has a large influence on the overall stiffness of the structure, thus increasing its critical buckling load. Finally, it is seen that for a given plate thickness and weld size, the critical buckling load decreases as overall panel size increases.

Results and Verification

The predicted mode shape and corresponding measured distorted shape for the laboratory mock-up panel is shown in Fig. 14. The predicted eigenmode correlates well with the observed shape. A direct comparison of the results between the predicted and measured distortion on the shipyard panel cannot be made, because the model contains only one stiffener while the measured data are for a panel with all three longitudinal stiffeners welded in place. However, comparison of the first few predicted mode shapes with the actual panel data shows that the fourth mode is dominant. The

may be suppressed for a variety of reasons, including the weight of the panel and stiffeners and the restraining effects of the additional stiffeners. A comparison of the predicted fourth mode shape and the measured panel is given in Fig. 15.

The resulting applied welding loads are compared to the critical buckling loads to predict whether buckling should occur. If the driving force supplied by welding is greater than the structure's critical buckling load, buckling should be observed in the corresponding mock-ups. The results of this comparison, along with the observed results, are given in Table 1. Since buckling results in fairly large out-of-plane distortions, observation of the welded panels is deemed sufficient to determine if buckling has occurred. As seen in the table, the predictions of the methodology described here are in direct agreement with the observed results for all experimental cases.

Structural Model

The 3-D continuum model utilized in the preceding discussions is useful in predicting the critical buckling load for stiffened panels. However, in terms of a design tool, construction of the 3-D model is tedious and time consuming and does not lend itself to making quick changes to the geometry. Additionally, due to the requirement that the mesh be continuous, the element size in this area must be at least on the order of the weld fillet leg and stiffener web thickness. This leads to large models that require excessive run times.

In an effort to provide a more robust design tool, a model constructed of structural elements is utilized. The model uses shell elements for the plate and beam elements for the stiffener. The weld load is applied using truss elements. With these types of elements, geometric features such as plate thickness, stiffener web and flange lengths, stiffener web and flange thickness, and applied weld load area are not explicitly modeled, but instead are input as properties of the respective elements. A special feature in the ABAQUS beam section properties definition allows for the origin of the beam local cross-section axis to be placed anywhere on the beam symmetry line, allowing the in defining the beam elements (Ref. 26). The same nodes are also used to define the truss elements, making the only restriction on the model geometry be that a line of nodes corresponding to the location of the stiffener centerline be present. This modeling procedure is illustrated in Fig. 16.

Model Description

The finite element model developed for the laboratory mock-up panel is shown in Fig. 17. The simplicity of the model is obvious from the figure. The model contains 2400 shell elements (ABAQUS S8R5), 48 beam elements, and 48 truss elements (ABAQUS B32 and T3D3, respectively). Although approximately the same number of elements are used for the continuum model, the mesh density for the plate has been increased by approximately 25%. Additionally, the structural model contains only 7397 nodes as compared to 18,019 for the continuum model. Therefore, for the same number of elements, the structural model analysis is completed in approximately one-half the time.

Results

Applied and critical weld loads are determined in a manner similar to that used for the continuum model. The resulting AWL and CBL values are listed in Table 2. These values are somewhat higher than those predicted for the continuum model. These differences are attributed to the additional restraint built in the model by offsetting the beam elements. Modeling the stiffeners with shell elements also is expected to improve the results.

The ease with which the analysis input deck is modified to reflect the different configurations shown in Table 2 should be emphasized. To evaluate different weld sizes, it is only necessary to change one number in the input deck, that corresponding to the cross-sectional area of the truss. To change the plate thickness requires only slightly more effort, changing one value representing the shell thickness and also adjusting some constants associated with the stiffener to change the beam local axis and the height of the stiffener above the plate midplane.

Table 2 also compares the predictions based on the structural model to observed results. As with the continuum model, the predictions are in direct agreement with the observed results. No comparison between predicted and observed buckling is available for the 7/32-in. (5.5563-mm) plate, because no experiment is performed with this geometry.

To assess the effect of the stiffener, an eigenvalue solution is obtained with the beam elements representing the stiffener removed. For the 3/16-in. (4.7625-mm) weld, removing the stiffener decreases the CBL to 19,037 lb (84.68 kN). This is approximately one-half the value determined when the stiffener is included, showing the need to include the stiffener in the models.

Distortion Magnitude Prediction

An incremental large deflection analysis is performed on the model developed for the laboratory mock-up

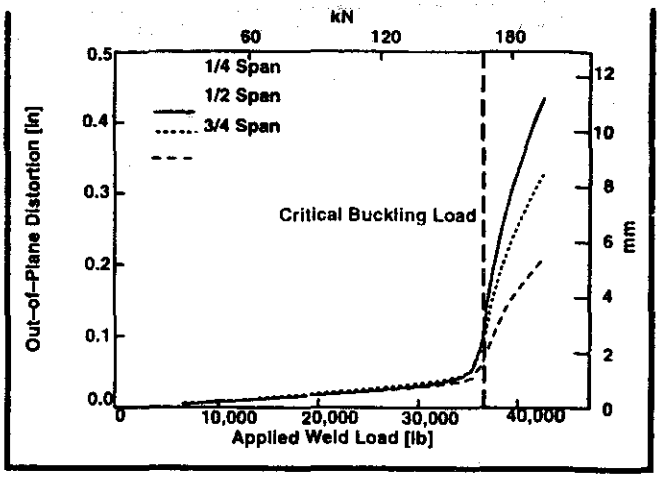

Fig. 18 — Predicted distortions at the transverse midplane for large deformation analysis.

Table 2 — The Comparison between the Predicted and Observed Results for Structural Model

Panel Size (ft)	Plate Thickness (in.)	Heat Input per Torch (kJ/in.)	Nominal Weld Size (in.)	Applied Weld Load AWL (lb)	Critical Buckling Load CBL (lb)	Buckling Predicted	Buckling Observed
4 × 4	3/16	7.88	1/8	28,082	39,865	No	No
4 × 4	3/16	10.2	5/32	37,296	39,895	No	No
4 × 4	3/16	18.2	3/16	48,011	39,925	Yes	Yes
4 × 4	7/32	18.2	3/16	48,011	56,911	No	—

panel — Fig. 1. Small imperfections, with a maximum imperfection equal to 1% of the plate thickness, are introduced to the geometry using the predicted mode shape from the eigenvalue solution. The introduction of the imperfections assures that there is always some response in the collapse mode(s) (Ref. 26). All other material properties and boundary conditions are identical to those used in the eigenvalue analysis. The thermal load is then applied incrementally up to and through the critical value.

Figure 18 shows the predicted out-of-plane deflection for the ¼, ½ and ¾ span locations at the transverse midplane of the plate. The figure shows that the response is linear until a load close to the CBL is reached. After this point, the deflection increases rapidly as the load is increased, indicating that the critical load has been exceeded. The critical load predicted by the large deflection analysis is slightly lower than the CBL, a consequence of seeding the model with the initial imperfections.

Examination of experimental results shows for the corresponding laboratory mock-up, the measured excursion along the transverse midplane between the ¼ and ¾ span points is approximately 0.211 in. (5.36 mm). As seen in Table 1, the applied welding load for this panel is 40,926 lb (182 kN). Examination of Fig. 18 shows that, at this load, the predicted excursion between these two locations is approximately 0.2 in. (5.08 mm), in good agreement with the measured value.

Large deflection analysis can also be used to incorporate the effects on welding into the overall response of the structure. An initial load step consisting of the weld load and appropriate boundary conditions can be made, followed by a second load step containing externally applied loads and modified boundary conditions (if necessary).

Summary

A methodology for predicting welding distortion and assessing the structural integrity of welded structures is presented. Thermo-elastic-plastic finite element analysis for welding simulation along with three-dimensional elastic and eigenvalue finite element analyses are performed to predict both the applied weld load and the structure's critical buckling load. The approach is particularized on evaluating buckling under longitudinal stresses and implemented on panel structures for shipbuilding.

The methodology presented is efficient and effective. The utilization of two-dimensional analyses for the welding simulations reduces the computational time and cost. Decoupling of the weld simulation from the 3-D analyses permits these analyses to be performed elastically, which allows for them to be solved quickly and efficiently. Utilizing structural elements in the 3-D analyses further enhances the efficiency of the model and allows for geometry changes to be implemented easily.

The predictive approach can be implemented at various stages in the design and production cycle. In the design stage, welding procedures can be set, and then various geometric configurations investigated. For example, to evaluate welding-induced buckling on panel structures, the plate thickness, stiffener size and stiffener spacing are altered until the structure's critical buckling load is greater than the applied load computed for the given welding procedure. The methodology can also be used to control distortion for established designs. In this case, the structure's critical buckling load is determined from a single eigenvalue analysis. Different welding processes and procedures are then examined to see if conditions can be established where the applied weld load is less than the established critical buckling load.

This method can also be used to assess the effectiveness of and establish the operating parameters for distortion mitigation techniques. Under certain conditions or constraints, it may not be possible to establish conditions where, under standard conditions, the applied weld load can be kept lower than the structure's critical buckling load. This could be the case for an established design that requires a minimum weld size or in cases where, due to weight limitations, it is not possible to increase the plate thickness sufficiently to avoid buckling. In these circumstances, the only way to avoid buckling is to employ proactive distortion mitigation techniques. For example, Michaleris and Sun (Ref. 27) demonstrate thermal tensioning to be an effective method for eliminating buckling in thin panel fabrication. Proper thermal tensioning parameters for various panel geometries can then be determined to ensure that buckling will be avoided. A similar methodology can be used for other proactive distortion mitigation techniques.

Acknowledgments

The authors would like to thank Carl C. Schultz, Jr., of Babcock & Wilcox for his contribution in the development of the weld load application technique.This work was funded by the Navy Joining Center project #93-04. The United States Government, Navy Joining Center and Edison Welding Institute make no warranties and assume no legal liability or responsibility for the accuracy, completeness or usefulness of the information disclosed in this report. Reference to commercial products, processes or services does not constitute or imply endorsement or recommendation.

References

1. Masubuchi, K. 1980. *Analysis of Welded Structures.* Pergamon Press. Oxford, U.K.

2. Terai, K. 1978. Study on prevention of welding deformation in thin-skin plate structures. *Kawasaki Technical Review,* No. 61, pp. 61–66.

3. Argyris, J. H., Szimmat, J., and Willam, K. J.1982. Computational aspects of welding stress analysis. *Computer Methods in Applied Mechanics and Engineering* 33:635–666.

4. Papazoglou, V. J., and Masubuchi, K. 1982. Numerical analysis of thermal stresses during welding including phase transformation effects. *Journal of Pressure Vessel Technology* 104:198–203.

5. Chakravarti, A., Malik, L. M., and Goldak, J. 1986. Prediction of distortion and residual stresses in panel welds. Symposium on Computer Modeling of Fabrication-Processes and Constitutive Behavior of Metals. Ottawa, Ontario, pp. 547–561.

6. Bibby, M. J., Goldak, J. A., Szyszkowicz, M. S., and Jefferson, I. 1988. Computational developments in the Watt transient microstructure algorithm. *Modeling of Casting and Welding Processes, IV,* eds. A. F. Giamei and G. J. Abbaschian, pp. 81–91. The Metals Society.

7. Free, A. J., and Goff, R. F. D. 1989. Predicting residual stresses in multi-pass weldments with the finite element method. *Computers and Structures* 32(2):365–378.

8. Teckiwal, P., and Mazumder, J. 1991. Transient and residual thermal strain-stress analysis of GMAW. *Journal of Engineering Materials and Technology* 113:336–343.

9. Ueda, Y., Murakawa, H., Gu, S. M., Okumoto, Y., and Kamichika, R. 1992. Simulation of welding deformation for precision ship assembling (Report I). In-plane deformation of butt welded plate. *Transactions of JWRI* 21(2):265–275.

10. Michaleris, P., Tortorelli, D. A., and Vidal, C. A. 1995. Analysis and optimization of weakly coupled thermo-elasto-plastic systems with applications to weldment design. *International Journal for Numerical Methods in Engineering* 38:1259–1285.

11. Watt, D. F., Coon, L., Bibby, M. J., Goldak, J., and Henwwod, C. 1988. An algorithm for modelling microstructural development in weld heat affected zones (Part A) Reaction kinetics. *Acta. Metall.* 36:3029–3035.

12. Oddy, A. S., Goldak, J. A., and McDill, J. M. J. Numerical analysis of transformation plasticity in 3D finite element analysis of welds. *European Journal of Mechanics,* A/Solids 9(3):253–263.

13. LeBLond, J. B. 1989. Mathematical modelling of transformation plasticity in steels II: Coupling with strain hardening phenomena. *International Journal of Plasticity* 5:573–591.

14. Das, S., Upadhya, G., Chandra, Kleinosky, M. J., and Tims, M. L. 1993. Finite element modeling of a single-pass GMA weldment. *Modeling of Casting, Welding and Ad-*

Piwonka, V. Voller and L. Katgerman, pp. 593–600. The Minerals & Metals Society.

15. Brown, S. B., and Song, H. 1992. Finite element simulation of welding of large structures. *Journal of Engineering for Industry* 114:441–451.

16. Daniewicz, S. R., McAninch, M. D., McFarland, B., and Knoll, D. 1993. Application of distortion control technology during fabrication of large offshore structures. AWS/ONRL International Conference on Modeling and Control of Joining Processes, Orlando, Fla.

17. Goldak, J., Chakravarti, A., and Bibby, M. 1984. A new finite element model for welding heat sources. *Metallurgical Transactions B* 15B:299–305.

18. Bathe, K. J. 1982. *Finite Element Procedures in Engineering Analysis*. Prentice Hall, Englewood Cliffs, N.J.

19. HKS, 1995. ABAQUS Theory Manual.

20. Conrardy, C., and Dull, R. 1996. Control of distortion and residual stresses in thin ship panels. Accepted for presentation at SNAME Ship Production Technicca Sympo-

21. The British Iron and Steel Research Association (eds.).1964. *Physical Constants of Some Commercial Steels at Elevated Temperatures*. Butterworths Scientific Publications, London, U.K.

22. Raymond, L. O., and Chipman, J. 1967. Thermodynamic functions of iron. *Trans. Metal. Soc. AIME* 239:630–633.

23. Mizukami, H., Mizukami, and Miyashita, Y. 1977. Mechanical properties of continuously cast steel at high temperatures. *Tetso-to-Hagane* (Iron and Steel), 63:46 (in Japanese).

24. Goldak, J. 1994. A predictive method for computing distortion due to welding in ship structures. Report submitted to Edison Welding Institute, Columbus, Ohio.

25. Goldak, J., Bibby, M., Moore, J., House, R., and Patel, B. 1986. Computer modeling of heat flow in welds. *Metallurgical Transactions B*, 17B:587–600.

26. Hibbitt, Karlsson & Sorensen, Inc. 1995. ABAQUS/Answers, Winter 1995. Providence, R.I.

27. Michaleris, P., and Sun, X. 1996. Finite element analysis of thermal tensioning techniques mitigating weld buckling distortion. *Residual Stresses in Design, Fabrication, Assessment and Repair*. ed. R.W. Warke, pp. 77–87, ASME PVP-vol 327.

PAPERS NEEDED FOR ASTM 12TH INTERNATIONAL SYMPOSIUM ON ZIRCONIUM IN THE NUCLEAR INDUSTRY

Papers are invited for the 12th International Symposium on Zirconium in the Nuclear Industry, sponsored by ASTM Committee B-10 on Reactive and Refractory Metals and Alloys. The symposium will be held June 15–18, 1998, in Toronto, Ontario, Canada.

The purpose of the symposium is to provide a forum for exchanging new information on preparation, fabrication, testing, development, characterization, and performance of zirconium-based materials in nuclear industry applications.

Whether submitting an abstract for an oral or a poster presentation, all prospective authors are requested to submit a title, a 250–300 word abstract, and an ASTM paper submittal form by May 15, 1997, to Dorothy Savini, Symposia Operations, ASTM, 100 Barr Harbor Dr., W. Conshohocken, PA 19428-2959 (610-832-9677). Paper submittal forms are available from Savini or from the symposium chairman. Authors are urged not to send abstracts by fax because often the copies do not reproduce clearly. A Special Technical Publication based on the symposium proceedings is anticipated by ASTM.

More information is available from Symposium Chairman George Sabol, Westinghouse NMD, Energy Center, Pittsburgh, PA 15230 (412-374-2273; Fax: 412-374-3282); or Editorial Chairman Gerry Moan, AECL, 2251 Speakman Drive, Mississauga, Ontario, Canada L5K 1B2 (905-823-9060, Ext. 3232; Fax: 905-823-0108).